

Pairing Vibrations Study with the Time-Dependent Hartree-Fock-Bogoliubov theory

B. Avez* and C. Simenel†
 CEA, Irfu, Service de Physique Nucléaire,
 Centre de Saclay, F-91191 Gif-sur-Yvette, France.

Ph. Chomaz
 GANIL (DSM-CEA/IN2P3-CNRS), B.P. 55027, F-14076 Caen cedex 5, France and
 CEA, Irfu/Dir, Centre de Saclay, F-91191 Gif-sur-Yvette, France.
 (Dated: March 7, 2022)

We study pairing vibrations in $^{18,20,22}\text{O}$ and $^{42,44,46}\text{Ca}$ nuclei solving the time-dependent Hartree-Fock-Bogoliubov equation in coordinate space with spherical symmetry. We use the SLy4 Skyrme functional in the normal part of the energy density functional and a local density dependent functional in its pairing part. Pairing vibrations are excited by two-neutron transfer operators. Strength distributions are obtained using the Fourier transform of the time-dependent response of two-neutron pair-transfer observables in the linear regime. Results are in overall agreement with quasiparticle random phase approximation calculations for Oxygen isotopes, though differences appear when increasing the neutron number. Both low lying pairing modes and giant pairing vibrations (GPV) are discussed. The GPV is observed in the Oxygen but not in the Calcium isotopes.

PACS numbers: 21.60.Jz, 24.30.Cz, 21.10.Re, 25.60.Je

I. INTRODUCTION

Energy density functional (EDF) approaches like the Skyrme-Hartree-Fock model [1, 2] have proved to be successful to describe bulk properties of nuclei over the nuclear chart [3]. Recent computer improvements allow large scale EDF calculations of nuclear structure [4, 5] and reactions [6, 7]. In these approaches, one restricts the many-body wave-functions to a subset of the Hilbert space on the one hand and guess a nuclear EDF on the other hand. A commonly used technique is to break symmetries to enrich the variational sub-space and improve the description of nuclear structure. As an example, breaking gauge invariance associated to particle number conservation yields the Hartree-Fock-Bogoliubov (HFB) formalism [8, 9, 10]. This technique allows for the description of superfluidity in ground states of open-shell nuclei.

Extensions to treat collective excitations in the presence of pairing correlations are possible in the framework of the Quasiparticle Random Phase Approximation (QRPA) which has been widely used in nuclear structure studies [11, 12, 13, 14, 15, 16, 17]. This approach and its zero pairing counterpart (RPA) give reasonable estimates of giant resonances though improvements are necessary to reproduce fine structures [18]. In fact, the QRPA can be obtained from the linearization of the time-dependent Hartree-Fock-Bogoliubov (TDHFB) equation which provides a self-consistent evolution of an independent quasiparticles state. There is a consistency requirement that QRPA and the static limit of TDHFB should

use the same effective interaction. This is a natural feature of TDHFB that the same EDF can be easily used in the static and dynamical calculations thanks to the structure of the TDHFB equation. This is not always the case in (Q)RPA calculations where spin-orbit and Coulomb parts of the residual interaction are often omitted (see discussion in [19] and references therein), which may affect collective modes [15, 20, 21, 22].

Unlike in condensed matter where, for instance, TDHFB has been applied to study dynamics of Bose-Einstein condensates [23, 24], explicit time evolutions of nuclei including pairing are sparse and usually limited to the BCS ansatz of superfluidity with simple functionals [25, 26, 27] or to simple systems [28]. Only recently, a numerical method of solving TDHFB with the Gogny interaction [29] has been proposed to study quadrupole oscillations using a harmonic oscillator basis [30].

At the limit where pairing is neglected, however, extensive calculations of nuclear dynamics have been performed using the time-dependent Hartree-Fock (TDHF) formalism introduced by Dirac in 1930 [31]. In this approach, one considers the dynamics of independent particles in a self-consistent mean-field generated by all the others. The use of Skyrme EDF [32] allowed recent realistic calculations of both collision mechanisms [6, 7, 33, 34, 35, 36, 37, 38] and giant resonances [19, 39, 40, 41]. For instance, TDHF has been used to study anharmonicities in collective motion which are beyond the RPA range of applications [39, 42]. It is then an appealing challenge to repeat these works using TDHFB to investigate the role of pairing correlations in nuclear dynamics. In particular, "How do they affect low-energy reaction mechanisms?" is still an open question. However, full three-dimensional TDHFB codes for collisions are still prohibitive at moment. For nuclear structure purposes, pairing vibrations and rotations [43, 44, 45] also demand theoretical inves-

*Electronic address: benoit.avez@cea.fr

†Electronic address: cedric.simenel@cea.fr

tigations to reach realistic predictions [46]. Of particular interest are high-lying pairing collective modes like giant pairing vibrations (GPV) [47]. These modes can be viewed as coherent sums of two-quasiparticle excitations across a major shell. They are probed by two-nucleon transfer reactions [48, 49]. The GPVs are still unobserved experimentally but they are experiencing a renewed interest since recent theoretical developments predicted that the use of radioactive ion beams could provide better conditions for their studies [50, 51, 52].

In this article, we solve for the first time the TDHFB equation with a full Skyrme functional in the normal part of the EDF and a local density dependent one in its pairing part. As a first application, we investigate pairing vibrations using the linear response theory. Our model is then equivalent to a fully consistent QRPA including spin-orbit and Coulomb interactions also in the particle-hole channel. In section II, we recall the TDHFB formalism and the choice of the EDF. We present in section III numerical implementations in spherical symmetry. Then, we discuss in section IV our choice of observables associated to pairing vibrations in the framework of the linear response theory. Finally, we present the results for $^{18,20,22}\text{O}$ and $^{42,44,46}\text{Ca}$ isotopes in section V before to conclude in section VI.

II. FORMALISM

A. TDHFB equation

The TDHFB equation can be derived starting from the action between an initial and final time t_i and t_f

$$S = \int_{t_i}^{t_f} dt \langle \Psi(t) | i\hbar \frac{\partial}{\partial t} - \hat{H} | \Psi(t) \rangle \quad (1)$$

and writing the variational principle $\delta S = 0$ in the subspace of quasiparticle vacua. For each state $|\Psi\rangle$ of this sub-space, one can find a basis of quasiparticle annihilators $\{\hat{\beta}\}$ such that $\hat{\beta}_\mu |\Psi\rangle = 0$ for all μ [44]. The latter can be related to the particle creation and annihilation operators $\{\hat{a}^\dagger, \hat{a}\}$ through the Bogoliubov transformation [10]

$$\hat{\beta}_\mu = \sum_\nu (U_{\nu\mu}^* \hat{a}_\nu + V_{\nu\mu}^* \hat{a}_\nu^\dagger) \quad (2)$$

where the matrices U and V are such that the quasiparticle operators $\{\hat{\beta}^\dagger, \hat{\beta}\}$ fulfill the canonical anti-commutation rules for fermions.

The variational principle leads to the TDHFB equation [53]

$$i\hbar \frac{\partial}{\partial t} \mathcal{R} = [\mathcal{H}, \mathcal{R}]. \quad (3)$$

The generalized one-body density matrix reads

$$\mathcal{R}(t) = \begin{pmatrix} \rho(t) & \kappa(t) \\ -\kappa^*(t) & 1 - \rho^*(t) \end{pmatrix}, \quad (4)$$

where $\rho_{\mu\nu} = \langle \psi | \hat{a}_\nu^\dagger \hat{a}_\mu | \psi \rangle$ are the matrix elements of the normal density and $\kappa_{\mu\nu} = \langle \psi | \hat{a}_\nu \hat{a}_\mu | \psi \rangle$ are the elements of the pairing tensor. The generalized one-body Hamiltonian \mathcal{H} has a block structure and can be written in terms of the Hartree-Fock (HF) Hamiltonian h and the pairing field Δ

$$\mathcal{H} = \begin{pmatrix} h & \Delta \\ -\Delta^* & -h^* \end{pmatrix}, \quad (5)$$

where

$$h_{\mu\nu} = \frac{\delta \mathcal{E}[\rho, \kappa, \kappa^*]}{\delta \rho_{\nu\mu}} \quad \text{and} \quad \Delta_{\mu\nu} = \frac{\delta \mathcal{E}[\rho, \kappa, \kappa^*]}{\delta \kappa_{\mu\nu}^*}. \quad (6)$$

In the above HFB formalism, the functional $\mathcal{E}[\rho, \kappa, \kappa^*]$ is the expectation value of the exact Hamiltonian \hat{H} on the quasiparticle vacuum $|\Psi\rangle$.

A more practical form of the TDHFB equation is found by recasting these equations in terms of the quasiparticle components U and V introduced in Eq. (2)

$$i\hbar \frac{\partial}{\partial t} \begin{pmatrix} U_{\nu\mu} \\ V_{\nu\mu} \end{pmatrix} = \sum_\eta \begin{pmatrix} h_{\nu\eta} & \Delta_{\nu\eta} \\ -\Delta_{\nu\eta}^* & -h_{\nu\eta}^* \end{pmatrix} \begin{pmatrix} U_{\eta\mu} \\ V_{\eta\mu} \end{pmatrix}. \quad (7)$$

B. EDF approach

In nuclear physics, the above formalism should be modified, in particular to take into account the short range repulsive part of the nuclear interaction which makes the mean-field HFB approach irrelevant with the bare interaction. This is a reason why one generally replaces $\mathcal{E}[\rho, \kappa, \kappa^*]$ by an effective EDF fitted on nuclear properties without invoking directly the underlying exact Hamiltonian. Moreover, in the spirit of the density functional theory [54, 55, 56], this procedure allows to include many-body correlations.

Let us decompose the total energy into kinetic, Skyrme, Coulomb and pairing parts (see appendix A for an explicit expression of each component)

$$\mathcal{E} = \mathcal{E}_{kin} + \mathcal{E}_{Sk} + \mathcal{E}_{Coul} + \mathcal{E}_{pair}. \quad (8)$$

We choose the SLy4 parameterization [57] of the Skyrme functional [32] including time-odd densities [58]. The Coulomb energy includes direct and exchange terms. The latter is estimated using the Slater approximation [59]. The three first terms of Eq. (8) depend only on the normal densities. It is convenient to express the pairing energy \mathcal{E}_{pair} using the anomalous density

$$\tilde{\rho}_q(\mathbf{r}s, \mathbf{r}'s') = -2s' \kappa_q(\mathbf{r}s, \mathbf{r}' - s') \quad (9)$$

where s the projection of the spin and q the isospin. We use a local pairing functional (see, e.g., [2] and references therein)

$$\mathcal{E}_{pair} = \int d\mathbf{r} \frac{g}{4} \left[1 - \left(\frac{\rho_0(\mathbf{r})}{\rho_c} \right)^\gamma \right] \sum_q \tilde{\rho}_q^*(\mathbf{r}) \tilde{\rho}_q(\mathbf{r}) \quad (10)$$

where $\rho_q(\mathbf{r}) = \sum_s \rho_q(\mathbf{r}s, \mathbf{r}s)$ and $\tilde{\rho}_q(\mathbf{r}) = \sum_s \tilde{\rho}_q(\mathbf{r}s, \mathbf{r}s)$ are the local parts of the normal and anomalous densities with isospin q respectively, $\rho_0(\mathbf{r}) = \sum_q \rho_q(\mathbf{r})$ is the scalar-isoscalar density and g is the pairing coupling constant. The parameters ρ_c and γ are adjusted to generate pairing correlations preferably at the surface and/or in the bulk of the nucleus. Such a pairing scheme yields pairs of nucleons of the same isospin coupled to angular momentum zero. The simplicity of such an EDF made systematic three-dimensional HFB calculations over the whole nuclear chart possible [4, 5].

However, one has to face the divergence of local pairing densities [60]. It is then necessary either to regularize the equations by introducing a cutoff in the quasiparticle spectrum or eventually to perform a more complex renormalization scheme (for an example based on the Thomas-Fermi approximation, see [61, 62]).

In our calculations, we use a cutoff to regularize the TDHFB equation in a quasiparticle energy window of 80 MeV. This value allows two-quasiparticle excitations up to 160 MeV. The pairing parameters are fitted to reproduce a neutron spectral gap of 1.25 MeV in ^{120}Sn , the pairing acting both in the bulk and at the surface of the nucleus [63]. The obtained pairing coupling constant is $g = -275.25$ MeV with the parameters $\rho_c = 0.32 \text{ fm}^{-3}$ and $\gamma = 1$.

C. Particle number conservation

Due to the broken $U(1)$ gauge invariance associated to the particle number conservation, the HFB states are not eigenstate of the particle number operator \hat{N} . In static calculations, one adds a Lagrange multiplier λ , interpreted as a chemical potential, in order to fix the number of particles in average. In TDHFB dynamical simulations, however, the particle number obeys to

$$i\hbar \frac{\partial}{\partial t} \langle \hat{N} \rangle = \text{Tr} (\kappa \Delta^* - \Delta \kappa^*). \quad (11)$$

The definitions of Δ and $\tilde{\rho}$ in Eqs. (6) and (9) respectively, together with the choice of the pairing functional in Eq. (10) ensure that the right hand side of Eq. (11) vanishes. As a consequence, we do not need to enforce the conservation of the average number of particles with a chemical potential in the TDHFB equation.

Nevertheless, dropping this constraint in the dynamics induces a rotation of the Bogoliubov vacuum in gauge space [64]. In particular, the anomalous density of a stationary state will carry a phase $\exp(-2i\lambda t/\hbar)$. Then, the ground state expectation values of observables which are linear in the anomalous density will evolve in time. For instance, this is the case of the observable we use to study pairing vibrations (see Eq. (22)). The time-Fourier analysis of such an observable in the linear response theory (see section IV) will then contain a spurious peak at an energy $\hbar\omega = 2\lambda$. This is a manifestation of the Goldstone mode due to the broken symmetry associated to particle

number conservation. In QRPA calculations, it induces a spurious mode at zero energy. In order to avoid such a spurious mode in the linear response of TDHFB, we have to keep the static ground state chemical potential in the particle-hole field during the evolution. Finally, we note that the chemical potential λ is easy to compute only for nuclei with pairing. Thus we do not consider doubly magic nuclei as initial states in the present work.

III. NUMERICAL IMPLEMENTATION OF TDHFB

A. Spherical symmetry

The pairing functional defined in Eq. (10) couples only nucleons of the same isospin. We can then focus on semi-magical nuclei for which the spherical assumption is a good approximation. As a consequence, we solve the TDHFB equation using spherical symmetry.

Let us recast the problem with purely local fields in space, spin and isospin using this symmetry. The total many-body wave-function being rotational invariant, it is convenient to write the Bogoliubov transformation in the spherical basis using the standard notation for quantum numbers n, l, j and m (we omit the isospin q in the notation for simplicity)

$$\hat{\beta}_{nljm}^\dagger = \sum_k (\mathcal{V}_{kn}^{(ljm)} (-1)^{j-m} \hat{a}_{klj-m} + \mathcal{U}_{kn}^{(ljm)} \hat{a}_{kljm}^\dagger). \quad (12)$$

This definition ensures that the component m of these quasiparticle operators transforms under rotation as a tensor of rank j (see Eq. (8.79) of Ref. [53]).

We choose to solve the TDHFB equation in coordinate space using quasiparticle wave functions $U_\nu(\mathbf{r}s) \equiv U_{\mathbf{r}s,\nu}$ and $V_\nu(\mathbf{r}s) \equiv V_{\mathbf{r}s,\nu}$ defined as components of quasiparticle spinors

$$\begin{pmatrix} U_{nljm}(\mathbf{r}s) \\ V_{nljm}(\mathbf{r}s) \end{pmatrix} = \begin{pmatrix} \langle \mathbf{r}s | \hat{\beta}_{nljm}^\dagger | - \rangle \\ \langle - | \hat{\beta}_{nljm}^\dagger | \mathbf{r}s \rangle \end{pmatrix}, \quad (13)$$

where $|-\rangle$ is the particle vacuum. The standard decomposition of single particle orbitals in spherical coordinates writes $\langle \mathbf{r}s | nljm \rangle = R_{nlj}(r) \Omega_{ljms}(\theta\phi)$. The angular part is expressed in terms of Clebsch-Gordan coefficients and spherical harmonics $\Omega_{ljms} = \langle l(m-s) \frac{1}{2}s | jm \rangle Y_l^{m-s}$. Defining the radial quasiparticle wave functions $u_{njl}(r) = r \sum_k \mathcal{U}_{kn}^{(ljm)} R_{klj}(r)$ and $v_{njl}(r) = (-1)^{l+1} r \sum_k \mathcal{V}_{kn}^{(ljm)} R_{klj}^*(r)$, and using the property $\Omega_{lj-m}^* = -2s(-1)^{m+l-j} \Omega_{ljm-s}$, Eq. (13) becomes

$$\begin{pmatrix} U_{nljm}(\mathbf{r}s) \\ V_{nljm}(\mathbf{r}s) \end{pmatrix} = \frac{1}{r} \begin{pmatrix} u_{njl}(r) \Omega_{ljms}(\theta\phi) \\ 2s v_{njl}(r) \Omega_{ljm-s}(\theta\phi) \end{pmatrix}.$$

Following the same way as Dobaczewski *et al.* for the static HFB problem [65], we introduce the anomalous

field $\tilde{h}_q(\mathbf{r}s, \mathbf{r}'s') = \frac{\delta \mathcal{E}[\rho, \tilde{\rho}, \tilde{\rho}^*]}{\delta \tilde{\rho}_q^*(\mathbf{r}s, \mathbf{r}'s')}$ where only the pairing energy in Eq. (10) contributes. The EDF considered here contains only local densities (see appendix A). Therefore, the HF and anomalous fields are also local in space. Finally, it is possible to recast the TDHFB equation (7) as a set of Schroedinger like equations for the quasiparticle radial wave functions u and v

$$i\hbar \frac{\partial}{\partial t} \begin{pmatrix} u_{nlj} \\ v_{nlj} \end{pmatrix} = \begin{pmatrix} h_{lj} - \lambda & \tilde{h} \\ \tilde{h}^* & -h_{lj}^* + \lambda \end{pmatrix} \begin{pmatrix} u_{nlj} \\ v_{nlj} \end{pmatrix} \quad (14)$$

where λ is the chemical potential (see section II C). The expressions of the fields $h(r)$ and $\tilde{h}(r)$ and those of the various densities entering the EDF solved in spherical symmetry can be found in appendix A.

B. Computational details

The initial condition is obtained with the HFBRAD code [66] which solves the static HFB equation in spherical symmetry. We have constructed a time-dependent version of this code to solve the TDHFB equation with the functional described in section II B. The set of equations (14) is solved iteratively using a one-step predictor-corrector method [67] and a truncation of the time propagator

$$U(t, t + \delta t) = \exp\left(\frac{-i\delta t}{\hbar} \mathcal{H}(t + \delta t/2)\right) \quad (15)$$

at 4th order in δt .

Spatial derivatives are calculated in a discretized r -space using seven-points formula. The numerical accuracy of this method decreases increasing quasi-particle energy. As a consequence, this approximate derivation formula induces a small periodic variation of the HFB ground state (of the order of few tens of keV) due to high energy quasiparticles. We checked that this numerical artifact disappears if we develop the wave-functions on a constant step Lagrange mesh [68]. However, the latter method increases the numerical effort. The amplitude of these variations being linked to the mesh discretization, a mesh step of 0.15 fm has been found to ensure a good numerical precision with a reasonable computational effort. In particular, the energy is conserved up to 15 keV and deviations of the total number of particles are of the order of 10^{-7} in the present calculations. Though this latter value is one order of magnitude higher than in the TDHF case with the same numerical conditions, it is small enough to leave the observables of interest unaffected. Moreover, to avoid any unphysical contribution due to the approximate spatial derivative in the evolution of observables, we subtract from their expectation values the one obtained without external field. We checked that this procedure does not affect the physical content of the spectra presented in Sec. V.

Let us precise that we use hard box boundary conditions. The latter are not optimized for a proper treatment of the continuum because they lead to a discretized

quasiparticle spectrum. In addition, particles which are reflected on the boundaries of the box may interact with the nucleus and induce unphysical effects on the evolution of observables. This problem has been tackled in TDHF with the help of absorbing boundary conditions [19, 69]. However, we did not found this technique to be appropriate to treat the TDHFB continuum because of the non-vanishing asymptotic nature of the upper component of the quasiparticle wave-functions in Eq. (13) [65]. Though needed to refine description of unbound states [13], further improvements of the boundary conditions are beyond the scope of this exploratory work.

We consider nuclei with magic proton numbers and excitations acting on neutrons only. Then the calculations include pairing for neutrons only. The local pairing functional couples to high angular momenta and high energy quasiparticle states up to the energy cutoff of 80 MeV. In the calculations presented here, convergence of the static solutions have been obtained with a maximum total angular momentum for neutrons, for which the Bogoliubov transformation is achieved, of $j_c = 19/2$ (23/2) for Oxygen (Calcium) isotopes respectively. For Oxygen isotopes, a box radius 22.5 fm was used, in order to be in conditions as close as possible to the discrete QRPA results of Ref. [52]. Calculations for Calcium isotopes have been performed in a box of radius 30 fm.

Both the mesh step, through the derivation formulae, and the maximum angular momentum, through the centrifugal part of the kinetic operator, constrain very much the time step for which the calculations are stable. The adopted time step used in these calculations are 0.003 and 0.002 fm/c for Oxygen and Calcium isotopes respectively.

IV. LINEAR RESPONSE FRAMEWORK FOR PAIRING EXCITATIONS

A. Linear response theory

The linear response theory has been widely used with TDHF to study collective vibrations in nuclei [19, 39, 40, 41, 42, 70, 71, 72, 73, 74, 75, 76]. In this theory, one computes the time evolution of an observable

$$\Delta Q(t) = \langle \Psi(t) | \hat{Q} | \Psi(t) \rangle - \langle 0 | \hat{Q} | 0 \rangle \quad (16)$$

after an excitation induced by a small external potential $\hat{V}_{ext}(t) = \epsilon \hat{F} \xi(t)$ on the ground state $|0\rangle$ of the system. The parameter ϵ quantifies the intensity of the excitation. It has to be small enough to ensure the linear regime, i.e., the amplitude ΔQ_{max} of the response must be proportional to ϵ . In this study, the time dependence of the external potential is chosen to be a Dirac function $\xi(t) = \delta(t)$. The excitation is then equivalent to a boost applied on the ground state at the initial time

$$|\Psi(0)\rangle = e^{-i\epsilon \hat{F}/\hbar} |0\rangle. \quad (17)$$

The response $\Delta Q(t)$ to this excitation can be decomposed into various frequencies ω using

$$R_Q(\omega) = \frac{-\hbar}{\pi\epsilon} \int_0^\infty dt \Delta Q(t) \sin(\omega t). \quad (18)$$

In the particular case where the operators used for the excitation and the observations are the same, i.e., $\hat{F} = \hat{Q}$, Eq. (18) gives the strength distribution

$$R_F(\omega) = \sum_\alpha |\langle \alpha | \hat{F} | 0 \rangle|^2 \delta(\omega - \omega_\alpha) \quad (19)$$

where $\langle \alpha | \hat{F} | 0 \rangle$ is the transition amplitude between the ground state and the eigenstate $|\alpha\rangle$ of the Hamiltonian and $\hbar\omega_\alpha = E_\alpha - E_0$ is their energy difference.

When the excitation generates a transition to neighboring nuclei, E_0 and E_α are the energies of the ground and excited states of the final nucleus if one keeps the static chemical potential in the Hamiltonian (see section 10.1 of Ref. [53]). For instance, in the case of an addition of two nucleons on a nucleus of A nucleons, the energy of the mode reads $\hbar\omega_\alpha = E_\alpha^{(A+2)} - E_0^{(A+2)}$ where the ground state energy of the final nucleus is approximated by $E_0^{(A+2)} = E_0^{(A)} + 2\lambda$. Note that this energy may differ from the one obtained in a HFB calculation in the $A+2$ nucleus because of a possible rearrangement of the HFB field.

B. Application to pairing vibrations

Pairing vibrations of quantum numbers 0^+ can be excited by two-nucleon transfer reactions and have been studied in the small amplitude limit within the QRPA framework [52]. A Hermitean pair-transfer operator is given by [45]

$$\hat{F} = \sum_\nu \left(f_\nu \hat{a}_\nu^\dagger \hat{a}_{\bar{\nu}}^\dagger + f_\nu^* \hat{a}_{\bar{\nu}} \hat{a}_\nu \right) \quad (20)$$

where $\bar{\nu}$ denotes the time-reversed state of ν .

In this paper, we consider local excitations acting on neutrons only and, for the sake of simple notations, we do not write explicitly the isospin quantum number in the following. The pair-transfer operator then writes in coordinate space

$$\hat{F} = \int d\mathbf{r} f(\mathbf{r}) \left(\hat{a}_{\mathbf{r},\downarrow}^\dagger \hat{a}_{\mathbf{r},\uparrow}^\dagger + \hat{a}_{\mathbf{r},\uparrow} \hat{a}_{\mathbf{r},\downarrow} \right). \quad (21)$$

In this particular choice, the spatial distribution $f(\mathbf{r})$ is real. Using Eq. (9), the expectation value of \hat{F} simply writes

$$\langle \Psi(t) | \hat{F} | \Psi(t) \rangle = \frac{1}{2} \int d\mathbf{r} f(\mathbf{r}) (\tilde{\rho}_0(\mathbf{r}; t) + \tilde{\rho}_0^*(\mathbf{r}; t)) \quad (22)$$

where $\tilde{\rho}_0 = \sum_q \tilde{\rho}_q$.

To preserve spherical symmetry, we focus on monopole pairing modes, requiring a radial dependence only, i.e., $f(\mathbf{r}) \equiv f(r)$. We choose a Fermi-Dirac spatial distribution $f(r) = \left(1 + \exp\left(\frac{r-R_c}{d}\right)\right)^{-1}$ where the parameters $R_c = (1.27 A^{1/3} + 4)$ fm and $d = 0.5$ fm are chosen to allow for pair transfer on the whole nucleus on the one hand, and to remove unphysical high energy modes associated to pair creation outside of the nucleus on the other hand. Finally, this excitation may change the number of neutrons at the initial time. However, deviations are small in the present calculations ($\sim 10^{-3}$ neutrons).

We choose to follow the excitation operator \hat{F} itself to get its strength distribution defined in Eq. (19). We also decompose the excitation operator $\hat{F} = \sum_l \hat{F}_l$ into components of single particle angular momentum l

$$\begin{aligned} \hat{F}_l = & \sum_{nn'jm} \int d\mathbf{r} f(r) \langle nljm | \mathbf{r} \downarrow \rangle \langle n'lj(-m) | \mathbf{r} \uparrow \rangle \\ & \times \hat{a}_{nljm}^\dagger \hat{a}_{n'lj(-m)} + h.c. \end{aligned} \quad (23)$$

where *h.c.* denotes the *Hermitean conjugate* of the entire expression. Computing the response of the \hat{F}_l helps us interpret the spectra in terms of specific quasiparticle excitations.

We perform the calculations over a total time interval of $T = 1200$ fm/c. In order to minimize the effects of the time gate on the Fourier transforms, we follow the protocol given in Ref. [69], multiplying the observables by a time filter $\cos^2\left(\frac{\pi t}{2T}\right)$. This procedure induces an additional width of ~ 1 MeV.

V. RESULTS

In this section, two-neutron transfer in several nuclei is studied. To illustrate the method described in the previous section, we first detail the analysis in ^{18}O . Then, we present the results on neutron-rich Oxygen isotopes and on *f*-shell Calcium isotopes.

A. Detailed analysis on ^{18}O

We apply the boost of Eq. (17) in the linear regime on the HFB ground state of ^{18}O . The pair-transfer operator \hat{F} is defined in Eq. (21). The variation of the expectation value of \hat{F} , obtained from Eq. (22), is plotted in Fig. 1 as a function of time. We observe a complex evolution due to the excitation of several modes at different energies. We see in the inset that a strong variation of $\Delta F(t)$ occurs at early times because all modes are initially in phase [39].

The evolution in Fig. 1 is used to compute the strength distribution of \hat{F} according to Eq. (18) and using the time filter procedure described in the previous section. We have controlled that the extracted strength is independent of the excitation amplitude ϵ . The resulting spectrum is shown in Fig. 2(a) in solid line. We see two

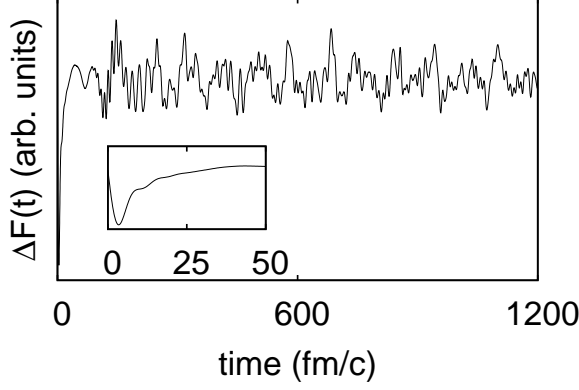


FIG. 1: Evolution of $\Delta F(t)$ after a pair transfer type excitation on ^{18}O . The inset shows the same quantity at early times.

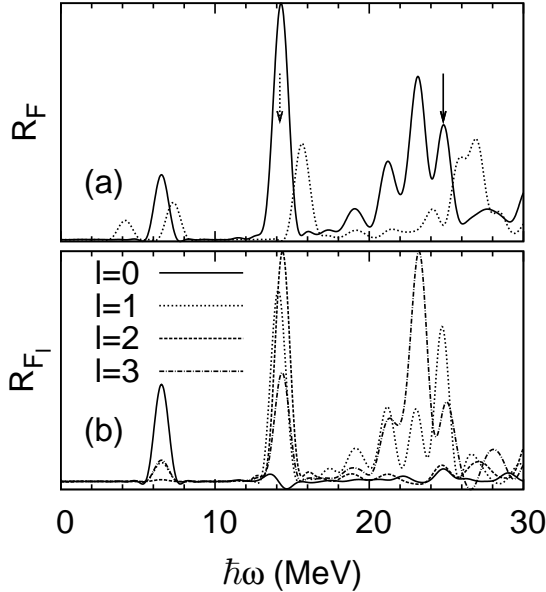


FIG. 2: Decomposition of the responses (in arbitrary units) into frequencies ω for a two-neutron pair transfer excitation in ^{18}O . (a) Strength distribution of \hat{F} obtained from TDHFB (solid line) and the unperturbed approximation (dotted line). The arrows indicate the $1p_{3/2}$ (solid) and $1p_{1/2}$ (dotted) deep hole states. (b) TDHFB responses of \hat{F}_l with $l = 0, 1, 2$ and 3 .

separated peaks at 6.5 and 14.3 MeV and several peaks between 20 and 26 MeV.

To understand the effect of the residual interaction which is included in TDHFB, we have computed the so-called unperturbed response to the pair transfer excitation. The latter is equivalent to Eq. (19) if one assumes that the states $|\alpha\rangle$ are two-quasiparticle excitations of the type $|\mu\nu\rangle = \hat{\beta}_\nu^\dagger \hat{\beta}_\mu^\dagger |0\rangle$ where $\hat{\beta}_\nu^\dagger$ creates a quasiparticle

eigenstate of the static HFB Hamiltonian on its ground state $|0\rangle$. In this approximation, the energy of the transition to the state $|\mu\nu\rangle$ is the sum of the quasiparticle energies $\hbar\omega_{\mu\nu} = e_\mu + e_\nu$. To allow for a quantitative comparison between the strength distributions obtained from TDHFB and unperturbed approximations, we compute the latter using the same time Fourier technique as for the TDHFB case. First, we determine the transition amplitudes $\langle\mu\nu|\hat{F}|0\rangle$ and then the time evolution of the observable $\hat{F} - \langle 0|\hat{F}|0\rangle$ within the unperturbed approximation. The latter reads

$$\Delta F^0(t) = \sum_{\mu\nu} |\langle\mu\nu|\hat{F}|0\rangle|^2 \sin(\omega_{\mu\nu}t). \quad (24)$$

Finally, we apply exactly the same procedure as for the TDHFB evolution to extract its strength distribution. The resulting unperturbed spectrum is represented by a dotted line in Fig. 2(a). We see clearly that the effect of the residual interaction is to increase the strength on the one hand and, on the other hand, to shift down the positions of the peaks.

To get a deeper insight into the nature of the peaks, we decompose the response into components of the single particle orbital momentum l using the observables \hat{F}_l defined in Eq. (23). The response for $l = 0, 1, 2$ and 3 are plotted in Fig. 2(b). These spectra, together with the quasiparticle HFB spectrum, allow us to characterize the peaks in terms of dominating two-quasiparticle excitations. As one can see in Fig. 2(b), the first peak located at 6.5 MeV is associated to the $l = 0$ component of \hat{F} . It corresponds mainly to a pair transfer toward the almost empty $2s_{1/2}$ orbitals.

The next peak, located at 14.3 MeV, is mainly a mixture of two contributions: the transfer of a pair towards $1d_{3/2}$ orbitals and the removal of the $1p_{1/2}$ occupied neutrons indicated by a dotted arrow in Fig. 2(a). The fact that these two modes have the same energy is fortuitous. (This is also the case at the unperturbed level.) As we will see later, they are well separated in the other Oxygen isotopes. We also see in Fig. 2(b) that there is a $l = 3$ contribution to this peak due to a coupling to $f_{7/2}$ orbitals in the continuum.

Let us now focus on the group of peaks at higher energies. As one can see in Fig. 2(b), they are mostly populated by $l = 1$ and 3 components. In fact, the peaks between 20 and 24 MeV are mainly associated to the excitation of $f_{7/2}$ quasiparticle resonant states while the peak at 24.7 MeV, indicated by a solid arrow in Fig. 2(a), corresponds to the deep hole $1p_{3/2}$ state. Except for the latter contribution, which is due to the removal of two occupied neutrons, these peaks belong to the GPV [52]. Indeed, they correspond to excitations of resonant states belonging to the next major shell and the enhancement of the strength as compared to the unperturbed spectrum is a sign of their collectivity [45].

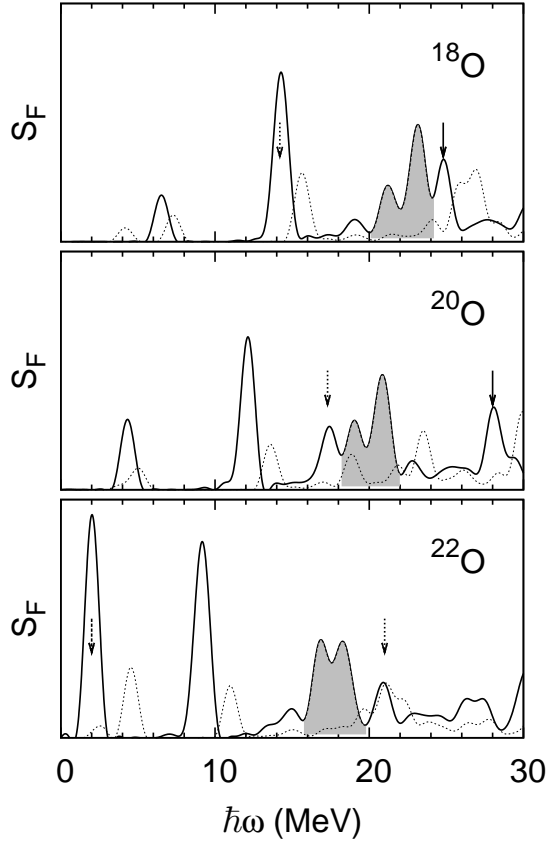


FIG. 3: Strength distributions of the two-neutron transfer operator \hat{F} for $^{18,20,22}\text{O}$ (in arbitrary units with the same scale on each plot). TDHFB results (solid lines) and the unperturbed approximation (dotted lines) are shown. The arrows indicate the $1p_{3/2}$ (solid) and $1p_{1/2}$ (dotted) deep hole states and the $1d_{5/2}$ (dashed) pair removal. The filled regions correspond to GPV candidates (see text).

B. neutron-rich Oxygen isotopes

In addition to ^{18}O , we also studied two-neutron pair transfer in $^{20,22}\text{O}$ nuclei. The spectra are shown in Fig. 3 while the energies and most important quasiparticle contributions to the main peaks are summarized in table I. Comparing strength distributions obtained from TDHFB (solid lines) with the unperturbed approximation (dotted lines) in Fig. 3 leads to the same conclusions for all isotopes, i.e., an increase of the strength and a lowering of the peak energies due to the TDHFB residual interaction. We also see in Fig. 3 that the energies of the $1p_{3/2}$ and $1p_{1/2}$ deep-hole states increase with the number of neutrons. The $1p_{3/2}$ peak in ^{22}O is located outside of the figure at 31.3 MeV. The occupied single particle orbitals are indeed deeper as compared to the Fermi level when increasing the neutron number, corresponding to higher quasiparticle energies. We also note that transi-

TABLE I: Energies and main quasiparticle contributions of the most important peaks appearing in the strength distribution of the two-neutron pair transfer operator \hat{F} extracted from TDHFB calculations for various Oxygen isotopes. Numbers in parentheses are the centroids of the continuum-QRPA energies of Ref. [52]. Labels in brackets indicate two-neutron removal contributions.

nucleus	E (MeV)	main orbital contribution
^{18}O	6.5(6.5)	$2s_{1/2}$
	14.3(14)	$1d_{3/2}, [1p_{1/2}]$
	20-24(21.5)	$f_{7/2}$
	24.7	$[1p_{3/2}]$
^{20}O	4.3(4)	$2s_{1/2}$
	12.1(11)	$1d_{3/2}$
	17.5	$[1p_{1/2}]$
	18-22(19)	$f_{7/2}$
	28.0	$[1p_{3/2}]$
^{22}O	2.0	$2s_{1/2}, [1d_{5/2}]$
	9.2(8)	$1d_{3/2}$
	16-20(16)	$f_{7/2}$
	21.0	$[1p_{1/2}]$

tions associated to the $1d_{5/2}$ orbital appear only in the ^{22}O spectrum. This is due to the fact that the operator \hat{F} leaves the strongly paired levels almost unchanged [45], and then no significant strength is associated to addition and removal of nucleons into a partially occupied level at the Fermi surface. This is not the case in ^{22}O where the $1d_{5/2}$ single particle orbital is almost fully occupied.

Last but not least, we see that the GPV, indicated by a filled region, is present in the three isotopes with similar amplitudes. In all cases, the most important contributions to the GPV are the excitation of $f_{7/2}$ quasiparticle resonant states. In the present calculations, continuum states are discretized due to the finite size of the box, inducing a fragmentation of the GPV. We also note that the GPV and the other two-neutron additional modes, contrary to the removal ones, have a decreasing energy with the neutron number. This is due to the fact that the Fermi level is less deep for neutron-rich nuclei, which decreases the quasiparticle energy of states with small or zero occupation number.

Let us now compare the energies predicted by the present TDHFB calculations with the continuum-QRPA results of Khan *et al.* [52], also reported in table I. The latter have been computed for two-neutron additional modes only. Compared to QRPA results, TDHFB calculations globally predict slightly higher energies when going to more neutron-rich nuclei. In the GPV region, the centroid energies are 0.5, 1 and 2 MeV higher with TDHFB for $^{18,20,22}\text{O}$ respectively. However, this overall agreement can be considered as good in regard to the differences between the two approaches. Both calculations use the SLy4 Skyrme functional, but with different pair-

ing schemes. In the present work, we use a mixed volume-surface effective coupling. In addition, our calculations are performed in wide quasiparticle energy and angular momentum windows, with cutoff values $E_c = 80$ MeV and $j_c = 19/2$ respectively, while the QRPA calculations have been performed in smaller windows ($E_c = 50$ MeV and $j_c = 9/2$) with a surface type pairing functional. The parameters of the latter have been determined using a different prescription than ours [13], in particular to reproduce the trend of the experimental gap in neutron-rich Oxygen isotopes. Another possible source of discrepancies is the fact that the QRPA calculations of Ref. [52] do not take into account the Coulomb and spin-orbit parts of the residual interaction whereas the TDHFB approach uses the same EDF as the underlying HFB field. This assumption may induce a slight shift in the energy of collective modes [20, 21, 22].

C. Calcium isotopes

In this section we discuss two-neutron pair transfer on $^{42,44,46}\text{Ca}$. We have plotted in Fig. 4 the corresponding TDHFB strength distributions (solid lines). The spectra are roughly similar for the three isotopes. They exhibit several discrete transitions to bound states together with excitations of resonant two-quasiparticle states. The energy threshold for the latter can be estimated by twice the Fermi energy, i.e., $2E_F = 20.6$, 19.6 and 17.8 MeV for ^{42}Ca , ^{44}Ca and ^{46}Ca respectively.

We performed the same analysis as for the Oxygen isotopes, i.e., we decomposed the strength distribution in l -components which, together with the HFB quasiparticle spectra, helped us assign the main quasiparticle contributions to each peak. A summary of the results is given in table II where the transitions associated to the removal of two neutrons are indicated in brackets.

For the three isotopes, the lowest mode is interpreted in terms of the addition of a neutron pair in the $2p_{3/2}$ orbitals. In ^{42}Ca , an additional $l = 2$ quasiparticle component contributes to this mode and corresponds to the removal of a $1d_{3/2}$ neutron pair. As for Oxygen isotopes, the appearance of removal modes (in brackets in table II) together with additional modes at the same energy is fortuitous. In the Calcium isotopes, the removal modes are built of neutrons from the $s - d$ shell, the major shell below the Fermi energy. As expected, one finally notes that energies of the removal (resp. additional) modes increase (decrease) with the neutron number. Although 2 $g_{9/2}$ quasiparticles excitations are forbidden below the $2E_F$ threshold in the unperturbed spectrum, it gets mixed to the last bound 2 ($f_{5/2}$) quasiparticles excitation because of the residual interaction.

We have also plotted the unperturbed spectra in Fig. 4 (dotted lines). As in the case of Oxygen isotopes, we observe that the TDHFB residual interaction lowers the energies on the one hand and increases the strength on the other hand, though this second effect is less pronounced

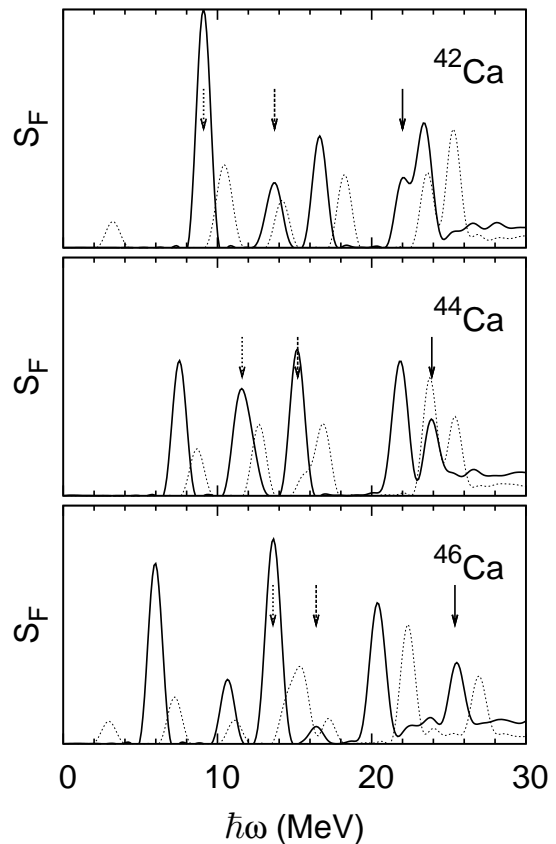


FIG. 4: Strength distributions of the two-neutron pair transfer operator \hat{F} for $^{42,44,46}\text{Ca}$ (in arbitrary units with the same scale on each plot). TDHFB results (solid lines) and the unperturbed approximation (dotted lines) are shown. The arrows indicate the $1d_{5/2}$ (solid), $2s_{1/2}$ (dashed) and $1d_{3/2}$ (dotted) two deep-hole states.

in the high energy part of the spectra. Here, the pairing residual interaction is not strong enough to gather high energy states together and to generate a well identified collective pairing vibration in the continuum. In a pure independent particles shell model picture, the last occupied neutron level of these Calcium isotopes is the $1f_{7/2}$ orbital. Then, one expects the GPV to be built mainly on low-lying $g_{9/2}$ resonant quasiparticle states. However, as we clearly see in Fig. 4, the strength associated to the two-quasiparticle excitation of $g_{9/2}$ levels, located at 23.4, 22.1 and 20.8 MeV for ^{42}Ca , ^{44}Ca and ^{46}Ca respectively, is only slightly enhanced by the TDHFB residual interaction. We checked that employing other parameterizations of the spatial distribution $f(r)$ of the excitation operator in Eq. (21) does not alter these conclusions. We note that this lack of collectivity of the $g_{9/2}$ has already been observed in hole pairing giant resonances studies within a more schematic formalism [77].

TABLE II: Energies and main quasiparticle contributions of the most important peaks appearing in the strength distribution of the two-neutron pair transfer operator \hat{F} extracted from TDHFB calculations for Calcium isotopes. Labels in brackets indicate two-neutron removal contributions.

nucleus	E (MeV)	main orbital contribution
^{42}Ca	9.1	$2p_{3/2}, [1d_{3/2}]$
	13.7	$2p_{1/2}, [2s_{1/2}]$
	16.6	$1f_{5/2}$
	22.0	$[1d_{5/2}]$
	23.4	$g_{9/2}$
^{44}Ca	7.5	$2p_{3/2}$
	11.6	$2p_{1/2}, [1d_{3/2}]$
	15.2	$1f_{5/2}, [2s_{1/2}]$
	22.1	$g_{9/2}$
	23.9	$[1d_{5/2}]$
^{46}Ca	6.0	$2p_{3/2}$
	10.7	$2p_{1/2}$
	13.6	$1f_{5/2}, [1d_{3/2}]$
	16.4	$[2s_{1/2}]$
	20.8	$g_{9/2}$
	25.4	$[1d_{5/2}]$

VI. CONCLUSION

We solved the TDHFB equation in coordinate space with spherical symmetry for the evolution of a single nucleus in an external field. For the normal part of the energy density functional, we used the SLy4 Skyrme functional. For its pairing part, we chose a local density dependent functional. Special care has been taken regarding the convergence of the static HFB solutions and the energy and particle number conservations in the TDHFB calculations.

As a first application, we studied 0^+ pairing modes excited by a two-neutron pair transfer type operator. The linear response theory has been used to compute the strength distributions of this operator in $^{18,20,22}\text{O}$ and $^{42,44,46}\text{Ca}$ nuclei. Both transitions to bound states and to the continuum are observed in all nuclei. In particular, the GPV is observed in all Oxygen isotopes whereas no significant enhancement of the strength due to dynamical pairing correlations appears in the continuum of the studied Calcium isotopes. In the latter, the $g_{9/2}$ quasiparticle excitations are not collective enough to generate a GPV.

A detailed comparison with previous QRPA calculations have been performed in the Oxygen isotopes. Though there is a good agreement for the most stable isotope, we find slightly higher energies for the pairing vibrations when going to more neutron-rich nuclei. Different pairing schemes and implementations of the residual interaction in both calculations are invoked to explain

these differences.

In addition, there is room for a better treatment of the continuum, for instance in the spirit of continuum-QRPA calculations, but such an improvement is not straightforward. Indeed, one cannot extrapolate the absorbing boundary conditions used in TDHF calculations to the TDHFB case because of the delocalized upper components of the Bogoliubov spinors.

Finally, TDHFB calculations are much more demanding in terms of computational time than standard TDHF calculations, by about two orders of magnitude in the one dimensional case. However, thanks to recent increase of computational power, some of the standard TDHF applications to nuclear structure and reactions should be repeated with the inclusion of dynamical pairing correlations in the framework of TDHFB.

Acknowledgments

We thank K. Bennaceur for his help on the HFBRAD code and the associated formalism. Discussions with M. Bender, T. Duguet, H. Flocard, E. Khan, D. Lacroix and V. Rotival are gratefully acknowledged. One of us (B.A.) also thanks R. Broglia and G. Ripka for useful discussions at the early stage of this work. Calculations have been performed at the Centre de Calcul CC-IN2P3.

APPENDIX A: DENSITIES AND FIELDS IN SPHERICAL SYMMETRY

Each energy term entering Eq. (8) can be written as a spatial integral of an energy density, i.e., $\mathcal{E} = \int d\mathbf{r} \mathcal{H}(\mathbf{r})$, which depends only on local densities and currents. For a spherically symmetric system, the densities entering the SLy4 and local density dependent pairing functionals are the radial part of the local particle $\rho_q(\mathbf{r})$, anomalous $\tilde{\rho}_q(\mathbf{r})$, kinetic $\tau_q(\mathbf{r})$, matter current $\mathbf{j}_q(\mathbf{r})$ and spin-orbit current $\mathbf{J}_q(\mathbf{r})$ (both oriented along the radial unit vector \mathbf{e}_r) densities of isospin q . Introducing the notation $\alpha \equiv \{n, l, j, q\}$, these densities write

$$\begin{aligned}
 \rho_q(\mathbf{r}) &= \sum_{nlj} K_j(r) |v_\alpha(r)|^2, \\
 \tilde{\rho}_q(\mathbf{r}) &= - \sum_{nlj} K_j(r) v_\alpha^*(r) u_\alpha(r), \\
 \tau_q(\mathbf{r}) &= \sum_{nlj} K_j(r) \left[\left| \left(\frac{\partial}{\partial r} - \frac{1}{r} \right) v_\alpha(r) \right|^2 \right. \\
 &\quad \left. + \frac{l(l+1)}{r^2} |v_\alpha(r)|^2 \right], \\
 \mathbf{j}_q(\mathbf{r}) &= \sum_{nlj} K_j(r) \text{Im} \left[v_\alpha(r) \left(\frac{\partial}{\partial r} - \frac{1}{r} \right) v_\alpha^*(r) \right] \mathbf{e}_r, \\
 \mathbf{J}_q(\mathbf{r}) &= \sum_{nlj} \frac{K_j(r)}{r} \left[j(j+1) - l(l+1) - \frac{3}{4} \right] |v_\alpha(r)|^2 \mathbf{e}_r,
 \end{aligned}$$

where $K_j(r) = \frac{2j+1}{4\pi r^2}$. We also define isoscalar densities as the sum of proton and neutron densities, e.g., $\rho_0(\mathbf{r}) = \rho_p(\mathbf{r}) + \rho_n(\mathbf{r})$. Omitting the dependence in \mathbf{r} to simplify the notations, the different parts of the functional can be written

$$\begin{aligned}\mathcal{H}_{kin} &= \frac{\hbar^2}{2m} \left(1 - \frac{1}{A}\right) \tau_0, \\ \mathcal{H}_{Sk} &= \sum_{k=n,p,0} \left\{ \left(C_k^\rho + C_k^{\rho^\alpha} \rho_0^\alpha\right) \rho_k^2 + C_k^{\Delta\rho} \rho_k \Delta\rho_k \right. \\ &\quad \left. + C_k^\tau (\rho_k \tau_k - \mathbf{j}_k^2) + C^{\mathbf{J}} \rho_k \nabla \cdot \mathbf{J}_k \right\}, \\ \mathcal{H}_{pair} &= \frac{g}{4} \left(1 - \left(\frac{\rho_0}{\rho_c}\right)^\gamma\right) \sum_{q=p,n} \tilde{\rho}_q^* \tilde{\rho}_q, \\ \mathcal{H}_{Coul} &= V_c^{dir} \rho_p - \frac{3}{4} e^2 \left(\frac{3}{\pi}\right)^{1/3} \rho_p^{4/3},\end{aligned}$$

where $V_c^{dir}(r) = \frac{e^2}{2} \int d\mathbf{r}' \frac{\rho_p(r')}{|\mathbf{r}-\mathbf{r}'|}$ is the direct Coulomb field. The factor $(1-1/A)$ in the kinetic part is the so-called one-body center of mass correction. The \mathbf{j}^2 term ensures Galilean invariance [78].

The coefficients C are related to the usual Skyrme coefficients by (see, e.g., [58])

$$\begin{aligned}C_0^\rho &= \frac{t_0}{2} \left(1 + \frac{x_0}{2}\right), \\ C_{n,p}^\rho &= -\frac{t_0}{2} \left(x_0 + \frac{1}{2}\right), \\ C_0^{\rho^\alpha} &= \frac{t_3}{12} \left(1 + \frac{x_3}{2}\right), \\ C_{n,p}^{\rho^\alpha} &= -\frac{t_3}{12} \left(x_3 + \frac{1}{2}\right), \\ C_0^\tau &= \frac{t_1}{4} \left(1 + \frac{x_1}{2}\right) + \frac{t_2}{4} \left(1 + \frac{x_2}{2}\right),\end{aligned}$$

$$\begin{aligned}C_{n,p}^\tau &= -\frac{t_1}{4} \left(x_1 + \frac{1}{2}\right) + \frac{t_2}{4} \left(x_2 + \frac{1}{2}\right), \\ C_0^{\Delta\rho} &= -\frac{3t_1}{16} \left(1 + \frac{x_1}{2}\right) + \frac{t_2}{16} \left(1 + \frac{x_2}{2}\right), \\ C_{n,p}^{\Delta\rho} &= \frac{3t_1}{16} \left(x_1 + \frac{1}{2}\right) + \frac{t_2}{16} \left(x_2 + \frac{1}{2}\right), \\ C^{\mathbf{J}} &= -\frac{W_0}{2}.\end{aligned}$$

The fields entering Eq. (14) write

$$\begin{aligned}h_{ljq}(r) &= -\frac{\partial}{\partial r} M_q(r) \frac{\partial}{\partial r} + I_q(r) \frac{\partial}{\partial r} + V_{ljq}(r) \\ \tilde{h}_q(r) &= \frac{g}{2} \left[1 - \left(\frac{\rho_0(r)}{\rho_c}\right)^\gamma\right] \tilde{\rho}_q(r)\end{aligned}$$

with

$$\begin{aligned}M_q &= \frac{\hbar^2}{2m} + C_0^\tau \rho_0 + C_q^\tau \rho_q \\ I_q &= 2i (C_0^\tau \mathbf{j}_0 + C_q^\tau \mathbf{j}_q) \cdot \mathbf{e}_r \\ V_{ljq} &= U_q + \frac{l(l+1)}{r^2} M_q + \frac{1}{r} \left(\frac{\partial}{\partial r} M_q\right) - \frac{I_q}{r} \\ &\quad - \frac{j(j+1) - l(l+1) - 3/4}{r} C^{\mathbf{J}} \left(\frac{\partial}{\partial r} (\rho_0 + \rho_q)\right), \\ U_q &= \sum_{k=q,0} \left[2 \left(C_k^\rho + C_k^{\rho^\alpha} \rho_0^\alpha\right) \rho_k \right. \\ &\quad \left. + \alpha C_k^{\rho^\alpha} \rho_0^{\alpha-1} (\rho_p^2 + \rho_n^2) + C_k^\tau \tau_k \right. \\ &\quad \left. + 2 C_k^{\Delta\rho} \Delta\rho_k + C^{\mathbf{J}} \nabla \cdot \mathbf{J}_k + i C_k^\tau \nabla \cdot \mathbf{j}_k \right] \\ &\quad - \frac{g}{4} \gamma \frac{\rho_0^{\gamma-1}}{\rho_c^\gamma} (|\tilde{\rho}_p|^2 + |\tilde{\rho}_n|^2).\end{aligned}$$

-
- [1] J. R. Stone and P.-G. Reinhard, Prog. Part. Nucl. Phys. **58**, 587 (2007).
[2] M. Bender, P.-H. Heenen, and P.-G. Reinhard, Rev. Mod. Phys. **75**, 121 (2003).
[3] D. Vautherin and D. M. Brink, Phys. Rev. C **5**, 626 (1972).
[4] M. Bender, G. F. Bertsch, and P.-H. Heenen, Phys. Rev. Lett. **94**, 102503 (2005).
[5] M. Bender, G. F. Bertsch, and P.-H. Heenen, Phys. Rev. C **73**, 034322 (2006).
[6] A. S. Umar and V. E. Oberacker, Phys. Rev. C **73**, 054607 (2006).
[7] C. Simenel and B. Avez, Int. J. Mod. Phys. E **17**, 31 (2008).
[8] D. R. Hartree, Proc. Cambridge Philos. Soc. **24**, 89 (1928).
[9] V. Fock, Z. Phys. A **61**, 126 (1930).
[10] N. Bogoliubov, Sov. Phys. JETP **7**, 41 (1958).
[11] J. Engel, M. Bender, J. Dobaczewski, W. Nazarewicz, and R. Surman, Phys. Rev. C **60**, 014302 (1999).
[12] M. Bender, J. Dobaczewski, J. Engel, and W. Nazarewicz, Phys. Rev. C **65**, 054322 (2002).
[13] E. Khan, N. Sandulescu, M. Grasso, and N. Van Giai, Phys. Rev. C **66**, 024309 (2002).
[14] S. Fracasso and G. Colo, Phys. Rev. C **72**, 064310 (2005).
[15] J. Terasaki, J. Engel, M. Bender, J. Dobaczewski, W. Nazarewicz, and M. Stoitsov, Phys. Rev. C **71**, 034310 (2005).
[16] J. Terasaki and J. Engel, Phys. Rev. C **74**, 044301 (2006).
[17] S. Péru and H. Goutte, Phys. Rev. C **77**, 044313 (2008).
[18] D. Lacroix, S. Ayik, and P. Chomaz, Prog. Part. Nucl. Phys. **52**, 497 (2004).
[19] T. Nakatsukasa and K. Yabana, Phys. Rev. C **71**, 024301 (2005).
[20] G. Colo and N. Van Giai, Nucl. Phys. A **731**, 15 (2004).
[21] S. Péru, J.-F. Berger, and P.-F. Bortignon, Eur. Phys. J. A **26**, 25 (2005).
[22] T. Sil, S. Shlomo, B. K. Agrawal, and P. G. Reinhard, Phys. Rev. C **73**, 034316 (2006).
[23] M. Holland, J. Park, and R. Walser, Phys. Rev. Lett. **86**, 1915 (2001).
[24] H. Buljan, M. Segev, and A. Vardi, Phys. Rev. Lett. **95**,

- 180401 (2005).
- [25] J. W. Negele, S. E. Koonin, P. Möller, J. R. Nix, and A. J. Sierk, Phys. Rev. C **17**, 1098 (1978).
 - [26] R. Y. Cusson and H. W. Meldner, Phys. Rev. Lett. **42**, 694 (1979).
 - [27] R. Y. Cusson, J. A. Maruhn, and H. Stöcker, Zeit. Phys. A **294**, 257 (1980).
 - [28] J. Blocki and H. Flocard, Nucl. Phys. **A273**, 45 (1976).
 - [29] J. Dechargé and D. Gogny, Phys. Rev. C **21**, 1568 (1980).
 - [30] Y. Hashimoto and K. Nodeki, arXiv : 0707.3083 [nucl-th] (2007); talk given at the FIDIPRO-JSPS Workshop on Energy Density Functionals in Nuclei, 25-27 Oct. 2007, Keuruselka, Jyväskylä (Finland).
 - [31] P. A. M. Dirac, Proc. Cambridge Philos. Soc. **26**, 376 (1930).
 - [32] T. Skyrme, Phil. Mag. **1**, 1043 (1956).
 - [33] P. Bonche, S. Koonin, and J. W. Negele, Phys. Rev. C **13**, 1226 (1976).
 - [34] J. W. Negele, Rev. Mod. Phys. **54**, 913 (1982).
 - [35] C. Simenel, P. Chomaz, and G. de France, Phys. Rev. Lett. **86**, 2971 (2001).
 - [36] C. Simenel, P. Chomaz, and G. de France, Phys. Rev. Lett. **93**, 102701 (2004).
 - [37] J. A. Maruhn, P.-G. Reinhard, P. D. Stevenson, and M. R. Strayer, Phys. Rev. C **74**, 027601 (2006).
 - [38] C. Simenel, P. Chomaz, and G. de France, Phys. Rev. C **76**, 024609 (2007).
 - [39] C. Simenel and P. Chomaz, Phys. Rev. C **68**, 024302 (2003).
 - [40] A. S. Umar and V. E. Oberacker, Phys. Rev. C **71**, 034314 (2005).
 - [41] J. A. Maruhn, P.-G. Reinhard, P. D. Stevenson, J. R. Stone, and M. R. Strayer, Phys. Rev. C **71**, 064328 (2005).
 - [42] P.-G. Reinhard, L. Guo, and J. A. Maruhn, Eur. Phys. J. A **32**, 19 (2007).
 - [43] A. Bohr and B. Mottelson, *Nuclear Structure* (2 vol., W.A. Benjamin, Inc., 1975).
 - [44] P. Ring and P. Schuck, *The Nuclear Many-Body Problem* (Springer Verlag, 1980).
 - [45] D. Bès and R. Broglia, Nucl. Phys. **A80**, 289 (1966).
 - [46] C. H. Dasso and M. I. Gallardo, Phys. Rev. C **74**, 014307 (2006).
 - [47] R. Broglia and D. Bès, Phys. Lett. **B69**, 129 (1977).
 - [48] G. Ripka and R. Padjen, Nucl. Phys. **A132**, 489 (1969).
 - [49] R. Broglia, O. Hansen, and C. Riedel, Advances in Nuclear Physics **6**, 287 (1973).
 - [50] L. Fortunato, W. von Oertzen, H. M. Sofia, and A. Vitturi, Eur. Phys. Jour. A **14**, 37 (2002).
 - [51] W. von Oertzen and A. Vitturi, Rep. Prog. Phys. **64**, 1247 (2001).
 - [52] E. Khan, N. Sandulescu, N. Van Giai, and M. Grasso, Phys. Rev. C **69**, 014314 (2004).
 - [53] J.-P. Blaizot and G. Ripka, *Quantum Theory of Finite Systems* (MIT Press, 1986).
 - [54] P. Hohenberg and W. Kohn, Phys. Rev. **136**, B864 (1964).
 - [55] W. Kohn and L. Sham, Phys. Rev. **140**, A1133 (1965).
 - [56] E. Runge and E. K. U. Gross, Phys. Rev. Lett. **52**, 997 (1984).
 - [57] E. Chabanat, P. Bonche, P. Haensel, J. Meyer, and R. Schaeffer, Nucl. Phys. **A635**, 231 (1998).
 - [58] P. Bonche, H. Flocard, and P.-H. Heenen, Nucl. Phys. **A467**, 115 (1987).
 - [59] J. W. Negele and D. Vautherin, Nucl. Phys. **A207**, 298 (1973).
 - [60] J. Dobaczewski, W. Nazarewicz, T. R. Werner, J. F. Berger, C. R. Chinn, and J. Dechargé, Phys. Rev. C **53**, 2809 (1996).
 - [61] G. Bruun, Y. Castin, R. Dum, and K. Burnett, Eur. Phys. J. D **7**, 433 (1999).
 - [62] A. Bulgac and Y. Yu, Phys. Rev. Lett. **88**, 042504 (2002).
 - [63] J. Dobaczewski, W. Nazarewicz, and P.-G. Reinhard, Nucl. Phys. **A693**, 361 (2001).
 - [64] A. Bulgac, Phys. Rev. C **41**, 2333 (1990).
 - [65] J. Dobaczewski, H. Flocard, and J. Treiner, Nucl. Phys. **A422**, 103 (1984).
 - [66] K. Bennaceur and J. Dobaczewski, Comp. Phys. Com. **168**, 96 (2005).
 - [67] H. Flocard, S. E. Koonin, and M. S. Weiss, Phys. Rev. C **17**, 1682 (1978).
 - [68] D. Baye, J. Phys. B **28**, 4399 (1995).
 - [69] P.-G. Reinhard, P. D. Stevenson, D. Almed, J. A. Maruhn, and M. R. Strayer, Phys. Rev. E **73**, 036709 (2006).
 - [70] J. Blocki and H. Flocard, Phys. Lett. **B85**, 163 (1979).
 - [71] S. Stringari and D. Vautherin, Phys. Lett. **B88**, 1 (1979).
 - [72] A. S. Umar and M. R. Strayer, Phys. Lett. **B171**, 353 (1986).
 - [73] P. Chomaz and N. Van Giai, Phys. Lett. **B189**, 375 (1987).
 - [74] M. V. C. R. Chinn, A. S. Umar, and M. R. Strayer, Phys. Rep. **264**, 107 (1996).
 - [75] D. Almed and P. D. Stevenson, J. Phys. G **31**, S1819 (2005).
 - [76] P. Stevenson, D. Almed, P.-G. Reinhard, and J. Maruhn, Nucl. Phys. **A788**, 343 (2007).
 - [77] M. Herzog, R. Liotta, and T. Verste, Phys. Lett. **B165**, 35 (1985).
 - [78] Y. Engel, D. Brink, K. Goeke, S. Krieger, and D. Vautherin, Nucl. Phys. **A249**, 215 (1975).